Journal of Materials Chemistry C

PAPER

View Article Online
View Journal

Cite this: DOI: 10.1039/c7tc01001j

On the chemically-assisted excitonic enhancement in environmentally-friendly solution dispersions of two-dimensional MoS_2 and WS_2

Dalal Fadil, Ridwan F. Hossain, Gustavo A. Saenz and Anupama B. Kaul *

Received 8th March 2017,
Accepted 4th April 2017

DOI: 10.1039/c7tc01001j

rsc.li/materials-c

Current rectifying p–n junction devices are demonstrated from solution exfoliated two-dimensional (2D) molybdenum disulfide (MoS_2), and excitonic effects are elucidated for solution dispersions of not only MoS_2, but also another refractory 2D sulfide, tungsten disulfide (WS_2). The excitonic enhancement effects are correlated to new solution chemistries using environmentally friendly terpineol. The role of sonication time and centrifugation are analyzed in the presence of terpineol with isopropyl alcohol and surfactant ethyl cellulose, where the red-shift in the excitonic peaks is correlated to the size distribution of the nanoparticles using optical interferometry. This was correlated to the data obtained using photoluminescence, Raman spectroscopy, scanning electron microscopy and particle size analysis which also yielded results that were consistent with this finding. The terpineol dispersion exhibits the least red-shift of 5 meV from the top to the bottom of the vial, in contrast to non-terpineol dispersions where the red-shift is calculated to be as high as 90 meV, indicating terpineol's effectiveness in exfoliating a larger population of mono-to few-layer nanomembranes. Analysis of the optical absorption spectra allows for the extraction of the energy band gap for MoS_2 and WS_2. These results clearly show evidence of quantum confinement effects in solution dispersions of chemically exfoliated 2D MoS_2 and WS_2 which can be harnessed for a wide variety of optoelectronic devices that are amenable to scalable and high-throughput synthesis routes, using environmentally friendly solution chemistries.

1. Introduction

Two-dimensional (2D) layered materials (LMs) such as graphene and transition metal dichalcogenides (TMDCs) have been the focus of intense research recently due to their interesting optical, electronic, thermal and mechanical properties that are paving the way for new device platforms.[1–3] For example, thin film transistors,[4] supercapacitors,[5] biosensors,[6] and a wide variety of other electronic, optoelectronic and sensing modalities have been enabled by 2DLMs.[7–9] The d-orbital conductivity of the transition metal M in the formation of the TMDC with stoichiometry MX_2, where X is a group VI chalcogen atom (S, Se or Te), gives some TMDCs interesting optical properties. Non-conventional antimonene and arsenene 2D semiconductors with tunable band gap have also been predicted and explored for optoelectronic devices.[10,11] In some 2DLMs, the band gap E_g typically increases with decreasing layer number, and a transition from indirect band gap to direct band gap is observed in the limit of monolayers. For example, TMDCs such as MoS_2 and WS_2 have E_g (indirect) $\sim$ 1.2 eV and 1.4 eV in the bulk, respectively, whereas E_g increases to 1.8–1.9 eV and 1.9–2.1 eV for monolayers, respectively, and is also a direct gap in this limit.[12,13] Moreover, light emission measurements conducted on MoS_2 and WS_2 in the visible regime are suggestive of excitonic effects emergent in these materials.[14,15] Such excitonic effects are presumed to arise when an electron (e) is promoted to the conduction band (CB), leaving a hole (h) in the valence band (VB) after the optical absorption of a photon with energy $E > E_g$. Given the strong attractive Coulombic interaction in the quantum confinement limit of 2D nanosheets, this e–h pair, or exciton, is bound together with relatively large binding energies at room temperature, and provides certain 2DLMs with unique optical and optoelectronic properties. While excitonic effects have been observed in mechanically exfoliated monolayers of 2D MoS_2,[12] as well as chemically dispersed solutions,[16,17] here we provide an in-depth analysis of excitonic and hot luminescence effects that are observed in solution-dispersed, chemically exfoliated 2D MoS_2 and WS_2 from bulk crystals using environmentally friendly and biodegradable terpineol (T). Terpineol not only acts as a stabilizer but also seems to play a role in the effective exfoliation of the bulk crystallites. Such solution-based approaches provide advantages in terms of scalability and high throughput synthesis routes, and the use of environmentally-friendly,

Department of Electrical and Computer Engineering, University of Texas at El Paso, El Paso, TX 79968, USA. E-mail: akaul@utep.edu

biodegradable materials makes such dispersions attractive for sustainability and additive manufacturing practices, for example with the use of ink jet printing, which results in little material waste. At the same time, these dispersions based on terpineol provide an avenue to access the unique optical and opto-electronic properties emergent in the quantum regime, as exemplified by the excitonic effects observed here, for the realization of high-performance devices, compared to mechanical exfoliation that is clearly not amenable to scalability.

Just as the weak van der Waals interaction between the layers in 2DLMs allows these materials to be mechanically exfoliated into individual layers from the bulk crystal with ease,[1,13,18] chemicals – in conjunction with mechanical agitation – can have a similar effect to shear the layers to yield nanosheets and even monolayers in solution.[19] This approach is versatile, low-cost and can provide a sustainable route to the production of 2D nanosheets for device applications, including opening up prospects for the realization of functional structures on flexible, light-weight or transparent substrates. In order to disperse the 2DLMs in solution, ultrasonication is a commonly used approach to separate the bulk crystal into 2D nanosheets through high-energy jets that provide mechanical agitation, concurrent to the chemical action engendered by the dispersion solvent. Besides the ultrasonication conditions (power, time, frequency, *etc.*), the choice of solvent is also an important factor in determining the effectiveness of the dispersions, where some organic solvents have been shown to have cohesive energies close to the interlayer energies of 2DLMs.[20]

In this work, we have provided an in-depth analysis of the excitonic effects emergent in 2D MoS_2, as well as the less studied WS_2 system for the first time, which is dispersed in isopropanol (IPA), and the role of ethyl cellulose (EC) as a surfactant, and terpineol (T) is also explored. After sonication, the samples are centrifuged as noted in prior work to further mass-separate the dispersion,[19,21–23] presumably leaving monolayers to few layer nanosheets at the top of the vial, while the thicker or bulk flakes appear at the bottom. From the optical absorption spectra we not only characterize the location of the excitonic peaks that are a signature of hot-luminescence effects in MoS_2 and WS_2, but also compare the difference in E_g values obtained for nanosheets from the top to the bottom of the vial, for the first time. Structural characterization to infer the layer number and particle size was performed using photoluminescence (PL), Raman spectroscopy, scanning electron microscopy (SEM) and laser interferometry. The particle size analysis yielded a distribution of particle size for the two populations: samples taken from the top and bottom of the vial. The electronic transport in 2D MoS_2 dispersions is also analyzed and compared to that in mechanically exfoliated MoS_2, from which p–n junction behavior is noted for solution dispersed MoS_2 on p-type Si substrates. We believe that in the solution dispersions of MoS_2 where the excitonic peaks are amplified, such as in the terpineol based samples, the ensuing electron transport measurements also reveal enhanced device figures of merit for p–n junction devices compared to dispersions without terpineol. The comprehensive optical and electronic characterization of solution dispersed 2DLMs, particularly using the environmentally friendly solutions discussed in this work, should lay the foundation for the design of high-performance electronic and optoelectronic devices in the future.

2. Results and discussion

The MoS_2 and WS_2 bulk crystals were dispersed in vials at a concentration of 5 mg mL^{-1}, as shown in Fig. 1, using a combination of solvent IPA, surfactant EC, and stabilizer T. In prior work, both EC and T have been known to minimize nanomembrane re-aggregation.[24] The specific dispersion conditions for samples S1, S2, S3, S4, S5 and S6 are provided in Table 1 at two

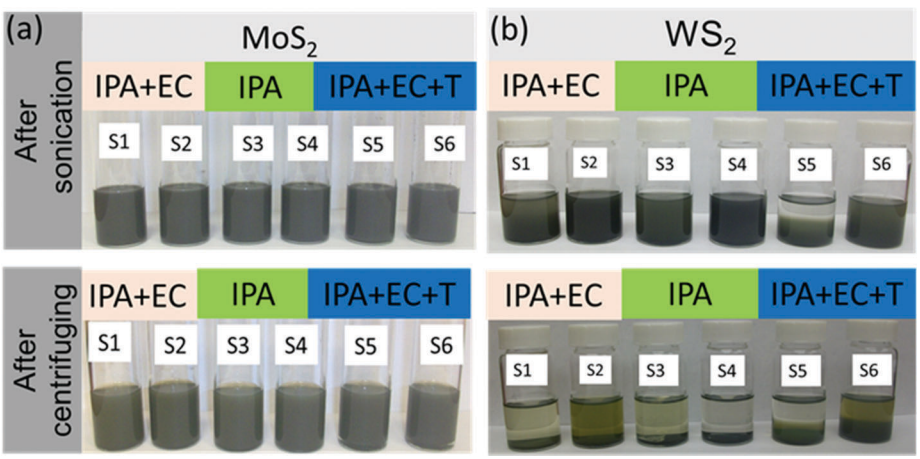

Fig. 1 Visual images of MoS_2 and WS_2 sample dispersions under the same conditions as noted for S1–S6. (a) MoS_2 after sonication in solvents (top) and after centrifugation in the same solvents at 2000 rpm (bottom). S1 and S2 correspond to dispersions prepared in IPA and EC at $t_{sonic} \sim 99$ min and 297 min, respectively. S3 and S4 correspond to dispersions prepared in IPA only at $t_{sonic} \sim 99$ min and 297 min, respectively. S5 and S6 correspond to dispersions prepared in IPA, EC and T at $t_{sonic} \sim 99$ min and 297 min, respectively (see Table 1). (b) WS_2 after sonication in solvents (top) and after centrifugation in the same solvents at 2000 rpm (bottom) under the same conditions as noted in (a) for MoS_2.

Table 1 Solution dispersions S1–S6 for MoS_2 and WS_2 at two sonication times (t_{sonic})

	Dispersion mixtures	t_{sonic} (min)
S1	2D material (50 mg) based on EC (5 mg) + IPA (10 mL)	99
S2	2D material (50 mg) based on EC (5 mg) + IPA (5 mL)	297
S3	2D material (50 mg) based on IPA (10 mL)	99
S4	2D material (50 mg) based on IPA (10 mL)	297
S5	2D material (50 mg) based on EC (5 mg) + IPA (5 mL) + T (5 mL)	99
S6	2D material (50 mg) based on EC (5 mg) + IPA (5 mL) + T (5 mL)	297

different sonication times t_{sonic}. Here, S1 and S2 represent dispersions formed using IPA and 3% EC surfactant at $t_{sonic} \sim 99$ min and 297 min, respectively; S3 and S4 are formed using IPA only at $t_{sonic} \sim 99$ min and 297 min, respectively; and S5 and S6 are formed using IPA, EC (3%) and T at a $t_{sonic} \sim 99$ min and 297 min, respectively. After sonication, the dispersions were centrifuged at 2000 rpm (805 rcf) for 30 min, and distinct differences could be seen in the MoS_2 and WS_2 solutions (Fig. 1). The WS_2 dispersions have a discernable color difference after centrifugation (Fig. 1b-bottom), which is likely related to the high degree of exfoliation and small lateral sizes of the nanosheets.[16,17] Interestingly, unlike the WS_2 dispersions, the separation and the change in color contrast in the MoS_2 samples (Fig. 1a-bottom) is less pronounced after centrifugation under the same dispersion conditions, which is likely to do with the higher mass of WS_2, increasing the likelihood of the WS_2 flakes settling at the bottom of the vial, unlike the lighter MoS_2 flakes which are likely to be more homogenously dispersed.

In order to investigate the optical properties of the 2D exfoliated solution dispersions, optical absorption spectra were obtained using a CARY UV-vis-NIR spectrophotometer. Given that there is a density band sedimentation gradient from top to bottom, we have analyzed the optical absorption characteristics of the dispersions taken from the two locations, *i.e.* the top and bottom of the vial, as shown in Fig. 2a and (b) for MoS_2 and WS_2, respectively. In the MoS_2 dispersions (Fig. 2a(i)–(iii)), at a fixed sonication time of 297 min (*i.e.* S2, S4 and S6), two distinct absorption peaks appear at energies $E_A \sim 1.83$ eV and $E_B \sim 2$ eV. As has been noted in prior work,[12,19,25] these peaks are the excitonic *A* and *B* peaks that occur at energies E_A and E_B, respectively, and are

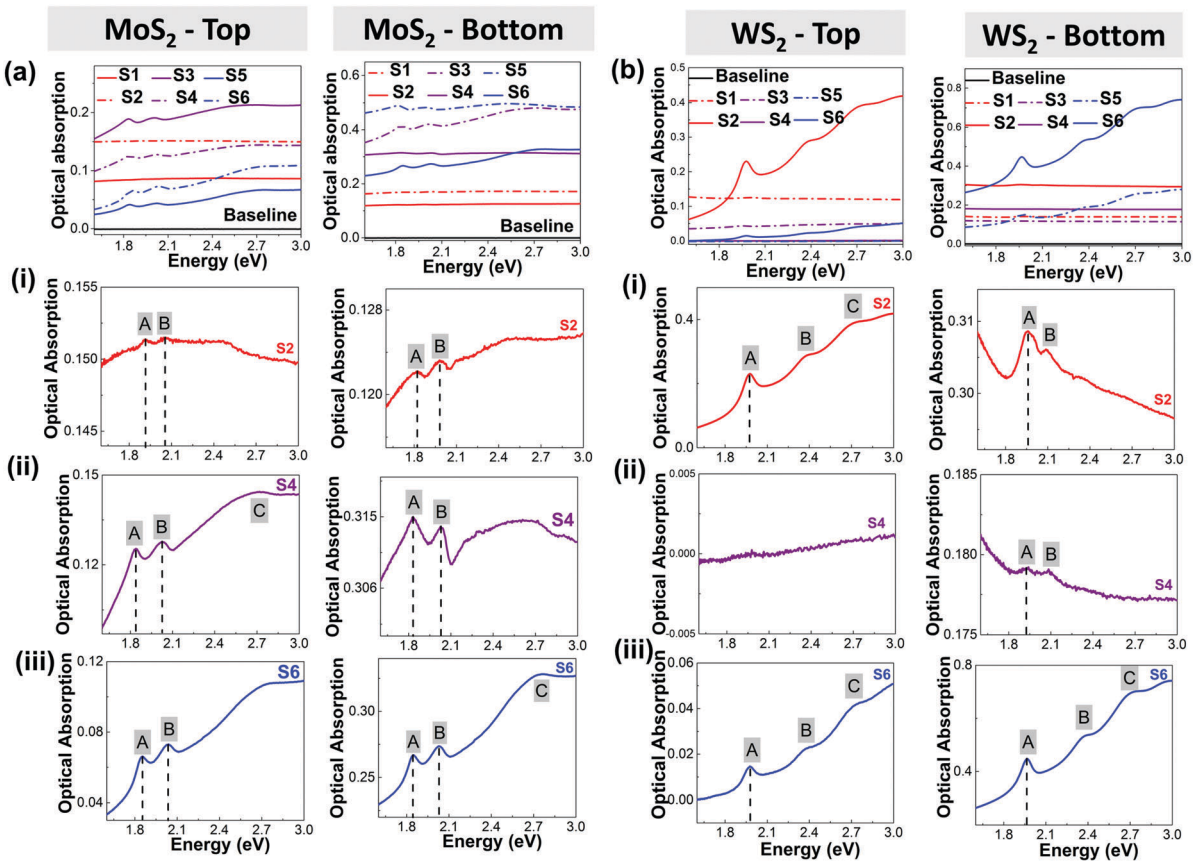

Fig. 2 Optical absorption spectra taken from the top and bottom of the vial for (a) MoS_2 and (b) WS_2. (a) (left) Samples taken from the top of the vial, and (right) bottom of the vial for MoS_2. (b) (left) Samples taken from the top of the vial, and (right) bottom of the vial for WS_2. The dashed line corresponds to a 99 min period of sonication and the continuous line corresponds to 297 min of sonication. (i–iii) represent more details of the absorption in the S2, S4, and S6 solutions.

an outcome of direct hot luminescence effects for our solution dispersed MoS_2. Here, direct gap transitions occur at the *K*-point of the Brillouin zone between the VB maxima and the CB minima. From the analysis of the data in Fig. 2a(i)–(iii), the value of the excitonic *A* peak measured for the solution at the top E_A(top) is greater than the excitonic *A* peak measured for the solution at the bottom E_A(bottom). Our analysis reveals that there is a red-shift in the excitonic peak location, as we go from top to bottom, *i.e.* $E_A(\text{top}) > E_A(\text{bottom})$ in most of the solution dispersions we have explored. For example, through our measurements $\Delta E_A = E_A(\text{top}) - E_A(\text{bottom})$ was calculated to be 90 meV, 11 meV and 5 meV for samples in the S2, S4 and S6 dispersions, respectively. The terpineol-based dispersion, S6, exhibited the least red-shift of 5 meV from the top to the bottom of the vial, in contrast to the non-terpineol dispersions, S2 and S4, where the red-shift is as high as 90 meV, indicating terpineol's effectiveness in exfoliating a larger population of mono- to few-layer nanomembranes. Moreover, Shi *et al.*[18] also observed a red-shift in E_A in bulk MoS_2 in comparison to mechanically exfoliated monolayer MoS_2. Our optical absorption spectra corroborate the quantum confinement induced effects that we have observed while noting the shift in the excitonic peak location that arises after centrifugation where the smaller and thinner flakes are at the top of the vial and the larger flakes are at the bottom.

Similarly, the WS_2 dispersions (Fig. 2b(i)–(iii)) show the excitonic *A* peak at $E_A \sim 1.97$ eV; interestingly no excitonic peaks are observed in the S4 dispersion at the top, and at the same time, very weak excitonic *A* and *B* peaks are seen at the bottom in this case. Additionally, the excitonic *B* peak in WS_2 appears at $E_B \sim 2.34$ eV which is weaker in amplitude when compared to the excitonic *B* peak in MoS_2 in samples S2, S4 and S6 for both the top and bottom cases (Fig. 2b(i)–(iii)). The locations of the E_A and E_B excitons from the literature are found to be 2.0 eV and 2.4 eV, respectively, for monolayers of mechanically exfoliated WS_2 which are comparable to the values we have obtained here in our solution dispersions of WS_2.[26] Under certain conditions, the excitonic C peak is also seen in WS_2 that has been attributed to Van Hove singularities which occur at critical points in the density of states, and can lead to strong optical absorption effects.[27] Here, we do indeed observe the excitonic C peak at $E_C \sim 2.72$ eV, which is only evident in the S2 (top) and S6 solution dispersions (top and bottom), corroborating the effective role of the EC + T in exfoliating and dispersing the 2DLMs. Interestingly, the optical images of the vials in Fig. 1b for WS_2 reveal that S2 and S6 samples are darker in color compared to the other dispersions (S1, S3, S4 and S5) after centrifugation, which may be an artifact of the strong optical absorption effects arising from the Van Hove singularities characteristic of the excitonic C peak in these specific dispersions. Moreover, $E_A(\text{top}) > E_A(\text{bottom})$ for the excitonic *A* peak of WS_2, where $\Delta E_A = E_A(\text{top}) - E_A(\text{bottom})$ was computed to be 12 meV for solution dispersions S2 and S6.

In general, from our analysis, it appears that the solution dispersions S5 and S6 formed using T appear to amplify the excitonic behavior of MoS_2, while similar effects are certainly noted for WS_2 in S6. The role of EC and T also seems to be important in enhancing the dispersibility of MoS_2 and WS_2, while at the same time minimizing re-agglomeration of the 2D nanoflakes.[15] In certain mixtures, *e.g.* S2 and S4 for WS_2 (*i.e.* Fig. 2b(i) and (ii) (right)), the absorbance of the bottom sample shows a reverse trend, in that the absorbance increases into the IR regime (lower energies) which may be due to defect states that arise in the mid-gap regime under these conditions. Another possibility is related to the poor exfoliation of the flakes which settle at the bottom.[16] A more detailed analysis is necessary to corroborate this however.

We have estimated the E_g of solution-dispersed MoS_2 and WS_2 by using the optical absorption spectra and fitting these spectra to the Tauc model.[28] This technique has been valuable in estimating the optical properties of other nanostructured materials, such as TiO_2 nanoparticles, ZnS quantum dots, and CdSe films.[29,30] In our implementation of this model to the solution dispersed MoS_2 and WS_2, the absorbance *A* from the optical spectra shown in Fig. 2 is used to plot $(\alpha h\gamma)^2$ as a function of *E*, where $\alpha = 2.303 \times A/d$ from the Lambert-Beer–Lambert law; here d =1 mm is the path length of the glass slide, h is Planck's constant, and γ is the incoming photon frequency in our spectrophotometer. As shown in Fig. 3a and b, E_g is then extracted from the *x*-intercept of the $(\alpha h\gamma)^2$ *versus* *E* plot. Using this model, we have also considered the scenario assuming an indirect band gap of our 2DLM dispersion, where the exponent n in $(\alpha h\gamma)^n$ is taken to be $\frac{1}{2}$.[31] However, this yielded a poor fit and the linear extrapolation did not intersect with the *E*-axis, lending support to the fact that our 2D MoS_2 and WS_2 dispersions indeed yield direct band gap optical absorption characteristics that are induced by quantum confinement effects.

Although Woomer *et al.* have shown a limitation of the Tauc model for the determination of E_g in 2D-black phosphorus,[32] in our fitting analysis we have conducted the fit outside of the regions in the *E*-axis where the *A* and *B* excitonic peaks emerge, and before the area where the C peak is presumed to arise, as shown in Fig. 3a and b. These data also indicate the reproducibility of the E_g calculation from the error bars calculated from the standard deviation of each mean gap energy value. This illustrates that the E_g(top) in general appears to be higher for the solution taken from the top of the vial for both MoS_2 and WS_2, compared to the E_g(bottom) calculation. This is in agreement with the notion that the nanosheets at the top will tend to be thinner after centrifugation, and hence $E_g(\text{top}) > E_g(\text{bottom})$ due to quantum confinement effects. Moreover, the magnitude of the mean variation $\Delta E_g = E_g(\text{top}) - E_g(\text{bottom})$ appears to be larger in WS_2 compared to MoS_2, as shown in Fig. 3c and d, which may be visualized by the distinct color difference of the vials after centrifugation for WS_2 in contrast to MoS_2, for which the color did not change to a large extent after centrifugation (Fig. 1).

The excitonic peak locations shown in Fig. 2 and E_g calculations in Fig. 3 were based on optical absorption spectroscopy measurements. Optical absorption spectroscopy in the UV-visible-NIR regime is a powerful technique and is commonly used to measure the absorption properties of 2D materials to highlight

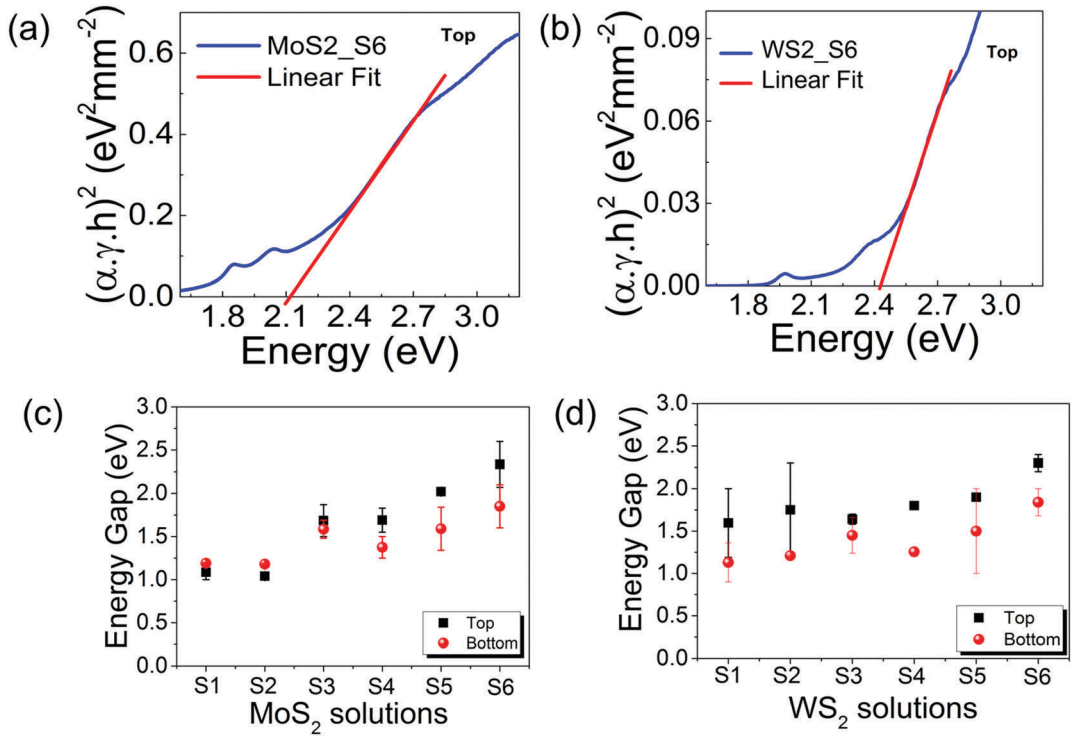

Fig. 3 Band gap E_g extraction from fitting to the Tauc model in the presence of excitonic peaks in solution S6 for (a) MoS_2 and (b) WS_2 dispersions. Tabulation of E_g obtained from the top and bottom of the solution dispersions for (c) MoS_2 and (d) WS_2 showing that E_g (top) generally tends to be larger than E_g (bottom) for most of the dispersions. Error bars represent the standard deviation of the mean value of the energy gap.

the existence of excitonic effects. For example, in early reports by Mak *et al.*,[12] optical absorption spectroscopy was used to study excitonic effects in mechanically exfoliated MoS_2, and follow-on work by Shi *et al.* in 2013[18] revealed the existence of excitons in suspended mono- and multilayer 2D materials using optical absorption spectroscopy, where red shift effects were also noted. We have also conducted photoluminescence (PL) measurements on our dispersions to support the findings obtained using optical absorption spectroscopy, as noted by the data in Fig. 2 and 3 for both MoS_2 and WS_2. We have conducted this PL analysis as a function of solvent chemistries S1 (without terpineol) and S6 (with terpineol) to examine excitonic effects in semiconducting MoS_2 and WS_2 using PL, where samples of the dispersions were taken from the top of the vial and compared to those obtained from the bottom of the vial.

Fig. 4(a)–(g) shows the PL, Raman spectroscopy, high resolution SEM and particle size data for MoS_2 and WS_2. In particular, in Fig. 4a and b, we provide the PL data corresponding to solution chemistry S1 (without Terpineol) and S6 (with terpineol) for MoS_2, respectively, where the black spectra represent data gathered for MoS_2 nanomembranes taken from the top of the vial, and the red spectra correspond to those taken from the bottom of the vial. These peaks are labelled as indirect *I* peaks for the bottom samples I_B, and the samples from the top I_T, while the *A* and *B* excitonic peaks, which represent direct band gap optical transitions, are labelled as A_T and A_B for *A*-excitonic peaks for the top and bottom, respectively, while B_T and B_B correspond to the *B*-excitonic peaks the for top and bottom, respectively. As is apparent from Fig. 4a, the peak coinciding with that of the monolayer emission *A*-peak,[33] we see a significant red shift from $A_T \sim 1.86$ eV and $A_B \sim 1.80$ eV, where broadening effects are also apparent for the A_B peak. This suggests that the dispersion chemistry S1 is not effective in exfoliating the material given the significant red-shift of $\sim$60 meV between the top and bottom (1.86–1.80 eV = 60 meV) which is consistent with the thicker material at the bottom approaching the bulk. Incidentally, the red-shift computed for non-terpineol based dispersions using optical absorption spectroscopy was computed to be 100 meV, in close agreement with the PL data. The indirect-gap PL peak at $I_B \sim I_T = 1.28$ eV becomes more pronounced as the thickness increases which is once again an indication that the material taken from the bottom is composed of thicker layers than the material taken from the top. In contrast, in Fig. 4b, which represents PL data obtained for solution chemistry S6 for MoS_2, terpineol appears to be effective in yielding a fewer layered material, even for samples taken from the bottom of the vial, where the red-shift effects are minimal since the locations of A_T and A_B occur at 1.87 eV. Moreover, there is also minimal broadening in the A_B peak in Fig. 4b, representing the monolayer emission peak.

Similarly for WS_2 where data are shown in Fig. 4c–d, the S1 sample in Fig. 4c indicates a large indirect I_B peak at 1.44 eV for the material taken from the bottom, characteristic of a thicker material. The *A*-excitonic peaks at the top and bottom occur at $A_T = 1.85$ eV and $A_B = 1.84$ eV, respectively, suggestive of a very small red-shift of 10 meV between the top and bottom.

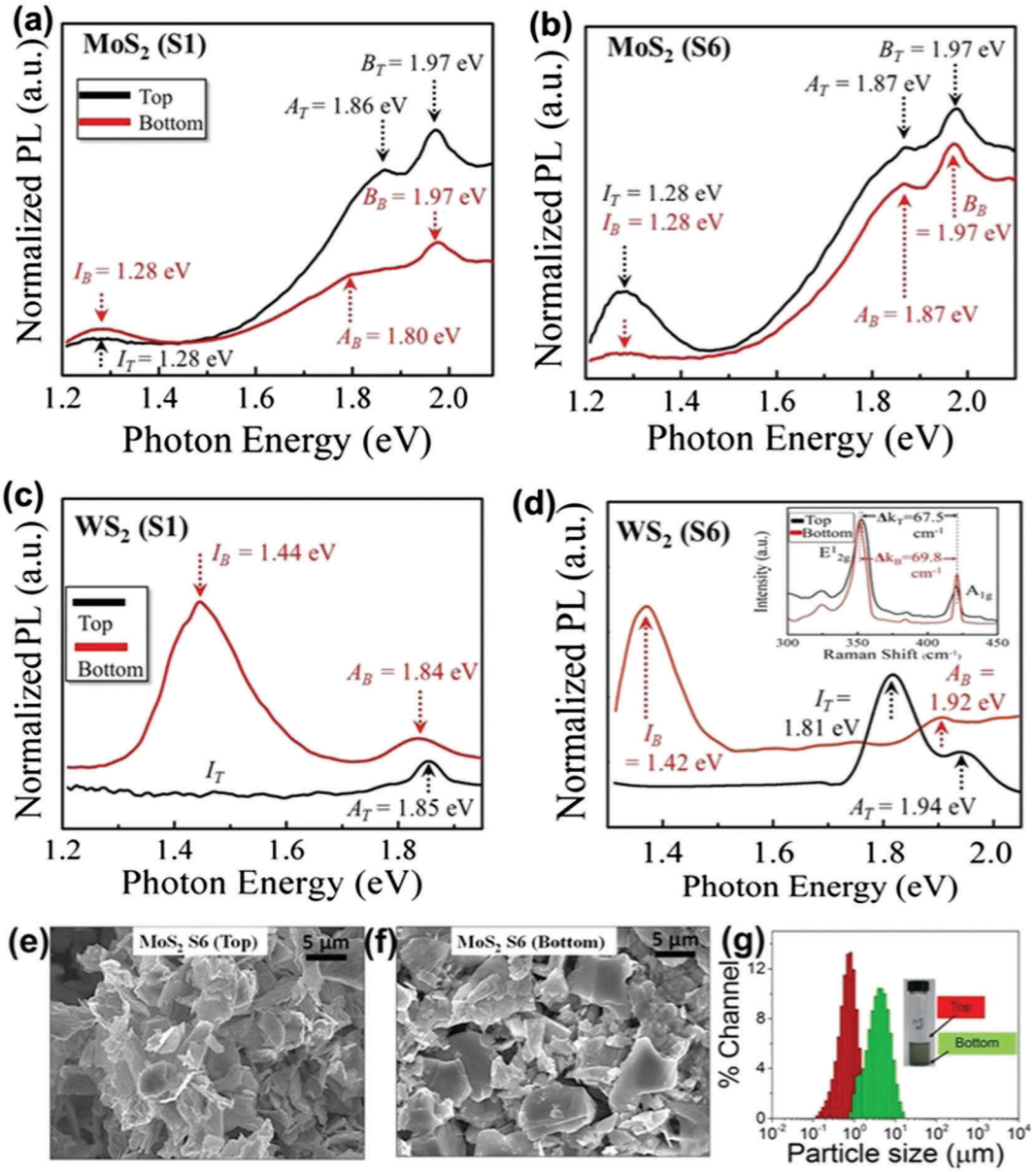

Fig. 4 (a) and (b) PL data corresponding to solution chemistries S1 (without terpineol) and S6 (with terpineol) for MoS_2, respectively, where the black spectra represent data gathered for MoS_2 nanomembranes taken from the top of the vial, and the red spectra correspond to materials taken from the bottom of the vial. For the peak coinciding with the monolayer emission A-peak,[33] we see a significant red shift from $A_T \sim 1.86$ eV and $A_B \sim 1.80$ eV, where broadening effects are also apparent for the A_B peak. This suggests that the dispersion chemistry S1 is not effective in exfoliating materials given the significant red-shift of $\sim$60 meV between the top and bottom which is consistent with the red-shift of 100 meV computed for non-terpineol based dispersion using optical absorption spectroscopy, in close agreement with the PL data. The indirect-gap PL peak at I_B–I_T = 1.28 eV becomes more pronounced as the thickness increases which is once again an indication that the material taken from the bottom is composed of thicker layers than the material taken from the top. (b) PL data obtained for S6 for MoS_2, where terpineol appears to be effective in yielding a fewer layered material, where the red-shift effects are minimal since the location of A_T and A_B occur at 1.87 eV. (c) and (d) PL data corresponding to solution chemistries S1 and S6 for WS_2, respectively. The A-excitonic peak at the top and bottom yields A_T = 1.85 eV whereas A_B = 1.84 eV, indicating that the material taken from the bottom is slightly red shifted compared to the material taken from the top. The inset in (d) shows the Raman spectra for WS_2 where $\Delta k_T \sim 67.5$ cm^{-1} between the out-of-plane A_{1g} mode and the in-plane E_{2g} mode for the material taken from the top, while $\Delta k_B \sim 69.8$ cm^{-1} for the material taken from the bottom. The $\Delta k_T \sim 67.5$ cm^{-1} is consistent with WS_2 being composed of bilayers.[34] High-resolution SEM imaging was conducted for MoS_2 for the material taken from the top of the vial in (e) and the morphology was compared to the material obtained from the bottom of the vial in (f) for S6. The SEM image in (f) clearly shows larger platelets, which are well above 5 μm in lateral dimensions, while the nanomembranes taken from the top of the vial shows the membranes to be thinner and smaller on average. (g) Particle size distribution of MoS_2 from the top and bottom for relative comparison. While the MoS_2 in this particular case was thermally treated for another experiment, a relative comparison shows distinct differences in particle size distribution for MoS_2 in a terpineol dispersion from the top and bottom, as indicated by the vial in the inset. The samples of MoS_2 taken from the top (red distribution) showed that the particle size has a Gaussian distribution with a mean particle size $S_{(top)} \sim 0.8$ μm (range = 0.1 to 3 μm), while for the samples taken from the bottom (green distribution), $S_{(bottom)} \sim 5.5$ μm (range = 1 to 20 μm).

The PL spectra for S6 in Fig. 4d shows the A_T peak occurring at a significantly larger energy ~1.94 eV, while the A_B peak is slightly red-shifted by ~20 meV since A_B occurs at ~1.92 eV, again suggestive of excitonic behavior occurring with thinner layers at the top. This is once again in close agreement with the optical absorption data reported for WS_2 in Fig. 2, where the red-shift was computed to be ~12 meV. The I_T peak was seen to be shifted toward higher energies at 1.81 eV compared to the I_B peak which was significantly red-shifted to 1.42 eV. The evolution of I_T to higher energies of ~1.81 eV is in excellent agreement with the PL data for WS_2 reported by Zhao *et al.*[34] and is suggestive of bilayer WS_2 membranes present in our terpineol based dispersions. The bi-layer configuration of our terpineol based dispersions is also corroborated by Raman spectroscopy analysis. The Raman spectra shown in the inset of Fig. 4d for WS_2 depicts the Raman shift $\Delta k_T \sim 67.5\ cm^{-1}$ between the out-of-plane A_{1g} mode and the in-plane E_{2g} mode for the material taken from the top, while $\Delta k_B \sim 69.8\ cm^{-1}$ for the material taken from the bottom. The $\Delta k_T \sim 67.5\ cm^{-1}$ is consistent with WS_2 being composed of bilayers. Zhao *et al.*[34] noted the evolution of electronic structure in atomically thin sheets of WS_2 where $\Delta k = 65.5\ cm^{-1}$, $68.3\ cm^{-1}$ and $69.2\ cm^{-1}$ corresponds to monolayer, bilayer and trilayer WS_2, respectively. In our case, the samples taken from the top of the vial show $\Delta k_T = 67.5\ cm^{-1}$, which clearly indicates the presence of bilayer WS_2 in the terpineol chemistry, again validating the promise of terpineol to exfoliate 2D WS_2 effectively.

Besides PL analysis which supports our optical absorption analysis data, we also conducted high-resolution SEM imaging for MoS_2 for materials taken from the top of the vial (Fig. 4e), and this morphology was compared to materials taken from the bottom of the vial (Fig. 4f) for S6. The SEM image in Fig. 4f clearly shows larger platelets, which are well above 5 μm in lateral dimensions, while the nanomembranes taken from the top of the vial are composed of smaller and thinner platelets, on average. This morphological change was also corroborated with a particle size measurement technique (Fig. 4g) that was conducted using dynamic laser scattering (MicroTac), where the particle size distribution of MoS_2 was measured for materials taken from the top and bottom, as illustrated in the inset of Fig. 4g. While MoS_2 in this particular case was thermally treated for another experiment, a relative comparison shows distinct differences in particle size distribution for MoS_2 in a terpineol dispersion from top and bottom. Samples of MoS_2 taken from the top (red distribution) showed that the particle size exhibited a Gaussian distribution with a mean particle size $S_{(top)} \sim 0.8$ μm (range = 0.1 to 3 μm), while for samples taken from the bottom (green distribution), $S_{(bottom)} \sim 5.5$ μm (range = 1 to 20 μm). This result is once again consistent with the optical absorption, PL, and SEM imaging analyses reported here.

As stated previously, the excitonic effects in 2D materials arise fundamentally from the large e–h pair binding energy that comes about from the strong Coulombic interaction in ultrathin 2D nanosheets. In fact, this was elucidated in one of the early reports dating back to the 1970's by Consadori *et al.*[35] who showed the enhancement occurring in the *A*-peak, *B*-peak and the A'-peak as mechanically exfoliated WSe_2 was thinned. This was attributed directly to the crystal size and quantum confinement effects operative in these systems. Subsequently, Mak *et al.*[12] and Splendiani *et al.*[36] built upon these concepts with PL and optical absorption spectroscopy analysis, where a strong enhancement in the PL intensity was seen for monolayer MoS_2, as compared to thicker films. In all of these seminal investigations nonetheless, the origin of excitonic effects in 2D materials are directly related to crystal size and geometrical confinement effects in the quantum limit.

While geometrical confinement in the quantum limit can amplify excitonic behavior in 2D layered materials, crystalline disorder, defects, or strain, as well as doping can also influence the characteristics of the excitons.[37–40] Intuitively, for a mechanically exfoliated monolayer 2D semiconducting crystal with a direct band gap one would expect a high PL yield. However, even for mechanically exfoliated monolayer MoS_2, the PL quantum yield was measured to be far lower $\sim 4 \times 10^{-3}$ than expected for such pristine mechanically exfoliated crystallites.[12] The origin of this low quantum yield has been discussed in the context of unintentional doping in the naturally derived crystals, where exciton formation may be suppressed with potential non-radiative recombination pathways. The enhancement in excitonic effects we observe with terpineol has thus far been discussed in the context of purely geometric crystal confinement effects, given terpineol's ability to more effectively shear the crystal planes in 2D MoS_2 and WS_2 to thinner platelets, where the Coulombic interactions will be enhanced compared to our reference dispersion based on IPA. As Coleman's[41] pioneering work on solution exfoliation points out, surface energy is an important parameter to gauge solvent efficacy. In fact modeling has shown that if the surface energy of the solvent is similar to that of the 2D material, the energy difference between the exfoliated and re-aggregated states will be very small, removing the driving force for re-aggregation.[41] Specifically, for solvents with surface tensions close to 40 mJ m^{-2}, the enthalpy of mixing is minimized for most 2D materials where the surface energies are ~60–70 mJ m^{-2}. Interestingly, the surface tension of terpineol (with EC) is ~42 mJ m^{-2} [42] and thus appears to be well matched to the ideal value predicted from modeling, in contrast to the surface tension for IPA which is far lower ~22 mJ m^{-2}.

Additionally, given terpineol's higher viscosity of ~40 cP at room temperature[24] compared to IPA (~2 cP), the rheological properties of the dispersions will also likely affect the degree of crystallinity, lattice distortion, defects and strain induced in the 2D materials, which can further suppress luminescence and excitonic effects. From our results, it is likely that given the better surface energy matching between terpineol and 2D MoS_2 and WS_2, coupled with its relatively higher viscosity even after mixing with IPA, the exfoliated nanosheets are likely composed of higher quality crystallites with fewer defects, which leads to more enhancement in excitonic effects in terpineol-based dispersions, compared to IPA, for example. The role of defects in quenching the luminescence properties of 2D solution dispersions was recently investigated by Eda and co-workers[25] where MoS_2 crystals exfoliated using Li intercalation in butyl lithium

solution and hexane yielded excitonic peaks that were less resolved. This suppression of the peaks was attributed to residual structural disorder from the remnant lattice distortion, and at the same time a progressive increase in the emission intensity was observed with increasing annealing temperature, suggesting that the crystalline order was largely restored. Zhao *et al.*[34] also discussed the Stokes shift and the line-width of the emission peak in WS_2 and other 2D selenides, which was once again related to the crystalline quality. This finding is in alignment with our data for the terpineol dispersions of MoS_2 for example, where we see minimal broadening in the A_B peak in Fig. 4b.

Finally, doping effects with our terpineol-based dispersions can also not be ruled out completely, particularly based on recent reports where doping was seen to influence the excitonic binding energy for MoS_2.[37] Similarly, Mouri *et al.*[43] showed an increase in the PL intensity in MoS_2 when p-type dopants derived from tetrafluorotetracyanoquinodimethane (F4TCNQ) and tetracyanoquinodimethane (TCNQ) were drop cast onto MoS_2. They discussed the excitonic enhancement in the context of exciton and charge carrier dynamics which gives rise to the formation of a many-body bound state, a charged exciton or trion, and a shift in the Fermi level was also induced. While doping effects may be operative in our solution dispersions of terpineol, more detailed characterization of the excitonic dynamics would be necessary to elucidate the exact mechanisms.

We have also conducted two-terminal electronic transport measurements for the 2D MoS_2 dispersions of S3 and S5 solutions that are drop cast onto SiO_2/Si substrates, as shown in Fig. 4. A mechanically exfoliated MoS_2 sample, denoted as m-MoS_2, was also prepared for comparative analysis, and this data is also shown in Fig. 4. In order to electrically contact the m-MoS_2 and the drop cast samples, MoS_2-S3 and MoS_2-S5, electrodes of Mo metal were sputtered onto SiO_2/Si substrates, at a thickness of 100 nm and patterned lithographically. For the m-MoS_2 sample, the mechanically exfoliated flakes were placed on top of the Mo contacts. For the drop cast MoS_2-S3 and MoS_2-S5 samples, annealing was conducted at 400 °C for 30 min in air. The *I–V* transport data were captured using a low-noise semiconductor parameter analyzer (Agilent 4156A) interfaced to a micro-manipulator probe stage, and tungsten (W) probe tips were used with a probe spacing of 16 μm, 18 μm, and 500 μm for the MoS_2-S3, MoS_2-S5, and m-MoS_2 samples, respectively. The inset in Fig. 4a depicts the transport characteristics of the m-MoS_2 sample measured over a wider voltage range prior to current saturation. From these data, we note that the magnitude of the current in S5 is larger than that of the S3 dispersion by more than 10× (*e.g.* at 5 V the current increases from 7 nA for S3 to 460 nA for S5) for similar device geometries. We believe that this enhancement in the electronic transport properties can be correlated to the role of the EC and T in yielding effective dispersions, and enhancing the excitonic peaks as also noted from the optical absorption spectra of MoS_2 for the S5 sample.

While there has been prior work on the field-effect-transistor (FET) behavior in chemically and mechanically exfoliated 2D materials,[4,44] analysis of the transport mechanism in drop cast 2D MoS_2 has been minimal to date, which we now discuss here in more detail. The *I–V* characteristics generally show an exponential conduction mechanism which can be expressed as $I(V) = I_0\,(\exp(\alpha V) - 1)$ for thermionic emission, where I_0 is the saturation current and α is a fitting parameter. The *I–V* data in Fig. 4a can be fitted to the Levenberg–Marquardt algorithm (least-squares method) when the measurement is reversible and noise is not taken into account. From the fitting of the *I–V* characteristics in the forward sweep mode of the MoS_2-S5 sample, we extract $I_0 \sim 2.5$ μA and $\alpha \sim 0.04$ (with $R^2 = 0.99949$). Other possible modes of conduction that exhibit an exponential dependence on the voltage include tunneling, generation–recombination mechanisms, and Schottky behavior,[45] but in our analysis we found that the thermionic emission provided a reasonable fit for the MoS_2-S5 sample. In the case of m-MoS_2 and MoS_2-S3 samples, a single fit to any one of the three exponential behaviors was not possible. In the latter two cases, the conduction mechanism seems to be a double-diode with two conduction mechanisms probably due to the Mo–MoS_2 Schottky contacts that exhibit no series resistance. Because the work function ϕ_0 of the W (probes) and Mo (electrodes) is ∼4.3–5.2 eV and ∼4.36–4.95 eV, respectively, which is close to $\phi_0 \sim$ 4.6–4.9 eV for MoS_2, we are unable to conclusively verify that a Schottky-barrier exists between MoS_2 and Mo. In prior work that considered Au and Ti contacts to MoS_2, factors such as annealing, contact metal deposition parameters, and surface cleanliness,[46] were all deemed important in controlling the interfacial work function to reduce the contact resistance in FET devices. Incidentally, Kang *et al.* reported on the formation of high-quality Mo–MoS_2 interfaces.[47]

Besides looking at the electronic transport characteristics of the 2D drop-cast dispersions of MoS_2, we also formed p–n junction devices where the drop-cast 2D MoS_2-S5 dispersion was placed on p-type Si substrates, as shown in Fig. 5b–d. Tungsten probes were used to measure the conductivity between the p-Si anode and the presumed n-type solution dispersed MoS_2 cathode. Here, the samples were annealed as previously described (at 400 °C for 30 min in air). As shown by the data in Fig. 5b–d, we elucidate the effect of solution chemistry on the device parameters, specifically leakage current I_0 and turn on voltage, V_T. The *I–V* data for solution chemistry S5, S1 and S6 are shown in Fig. 5b, c and d, respectively, where the inks were dispersed onto heavily doped p-type Si substrates. The figures of merit for the devices are summarized in (e) which indicate that the solution chemistry S6 yields the lowest V_T of ∼2 V, as compared to S5 which has a V_T of ∼4.87 V and S1 which has a $V_T \sim$ 11 V; the leakage currents for both of the terpineol derived solution chemistries, S5 and S6 yield $I_0 \sim$ on the order of 10–90 nA at 10 V, whereas the I_0 for S1 is ∼2 μA, which is approximately two orders of magnitude larger. All of these data once again validate the effectiveness of terpineol in enabling 2D dispersions that yield enhanced transport properties, which is also consistent with the enhanced excitonic effects observed in this particular solution chemistry. The transport behavior of our p–n junction devices and V_T values are similar to that reported by Jeong *et al.*[48] for MoS_2/p-GaN. Also in the reverse bias regime, Jeong *et al.*[48] did not see distinct rectification,

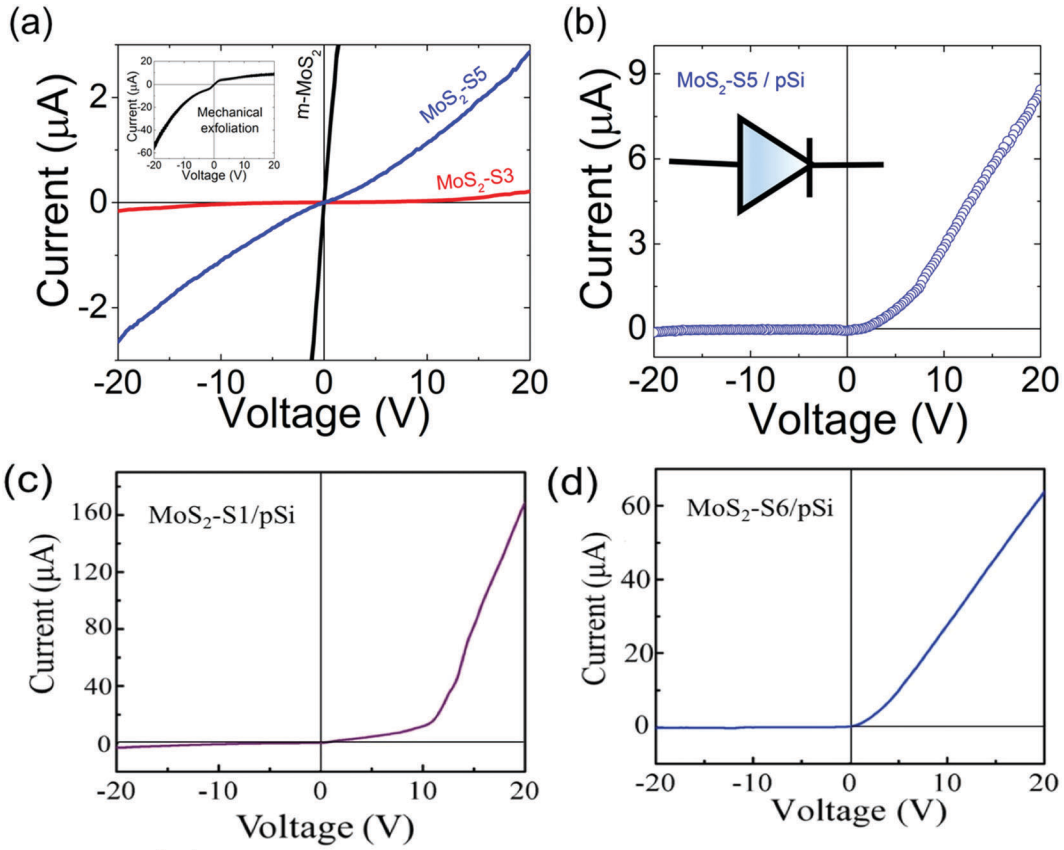

(e)

	Solution S1	Solution S5	Solution S6
I_o (@ 10 V)	1.7×10^{-6} A	1.8×10^{-8} A	8.8×10^{-8} A
V_T	11 V	4.87 V	2.08 V

Fig. 5 (a) $I-V$ characteristics of mechanically exfoliated m-MoS_2 and a drop cast MoS_2 dispersed under the conditions of S3 with Mo electrodes (red) and MoS_2 dispersed under the conditions of S5 (blue) deposited on SiO_2/Si. (b) $I-V$ characteristics of the p–n junction formed with MoS_2-S5 on doped p-Si substrates showing current rectification in the reverse bias regime with $V_T \sim 4.87$ V. The inset shows the symbol for a two-terminal current rectifying diode. (c) and (d) $I-V$ data for solution chemistries S1 and S6 where the inks were dispersed onto heavily doped p-type Si substrates, similar to the data obtained in (b). We see the effect of solution chemistry on the device parameters, specifically leakage current I_0 and turn on voltage, V_T. The figures of merit for the devices summarized in (e) indicate that the solution chemistry S6 yields the lowest V_T of ~2 V, as compared to S5 which has a turn on voltage of ~4.87 V and S1 with $V_T \sim 11$ V; the leakage currents for both of the terpineol derived solution chemistries S5 and S6 yield $I_0 \sim$ on the order of 10–90 nA, whereas the I_0 for S1 is ~2 μA, which is approximately two orders of magnitude larger. All of these data once again validate the effectiveness of terpineol in enabling 2D dispersions that yield enhanced transport properties, which is also consistent with the enhanced excitonic effects observed in this particular solution chemistry.

as we observe here in all three solution chemistries. The current behavior in our devices can be explained on the basis of the conventional p–n junction theory. In the forward bias regime (p-Si positively biased), the current scales exponentially with the height of potential barrier for $V > V_T$.[49] In the reverse bias regime (p-Si negatively biased), the depletion region increases and a weak leakage current flows through the junction in this reverse bias regime.

References

1 K. S. Novoselov, A. K. Geim, S. V. Morozov, D. Jiang, Y. Zhang, S. V. Dubonos, I. V. Grigorieva and A. A. Firsov, Electric field effect in atomically thin carbon films, *Science*, 2004, **306**(5696), 666–669.

2 A. K. Geim, Graphene: Status and Prospects, *Science*, 2009, **324**, 1530.

3 A. Castellanos-Gomez, Why all the fuss about 2D semiconductors? *Nat. Photonics*, 2016, **10**(4), 202–204.

4 Q. H. Wang, K. Kalantar-Zadeh, A. Kis, J. N. Coleman and M. S. Strano, Electronics and optoelectronics of two-dimensional transition metal dichalcogenides, *Nat. Nanotechnol.*, 2012, **7**(11), 699–712.

5 H. M. Jeong, J. W. Lee, W. H. Shin, Y. J. Choi, H. J. Shin, J. K. Kang and J. W. Choi, Nitrogen-doped graphene for high-performance ultracapacitors and the importance of

nitrogen-doped sites at basal planes, *Nano Lett.*, 2011, **11**(6), 2472–2477.

6 K. Kalantar-Zadeh and J. Z. Ou, Biosensors based on two-dimensional MoS_2, *ACS Sens.*, 2016, **1**(1), 5–16.

7 D. Jariwala, V. K. Sangwan, L. J. Lauhon, T. J. Marks and M. C. Hersam, Emerging device applications for semiconducting two-dimensional transition metal dichalcogenides, *ACS Nano*, 2014, **8**(2), 1102–1120.

8 S. Wu, Z. Zeng, Q. He, Z. Wang, S. J. Wang, Y. Du, Z. Yin, X. Sun, W. Chen and H. Zhang, Electrochemically Reduced Single-Layer MoS_2 Nanosheets: Characterization, Properties, and Sensing Applications, *Small*, 2012, **8**, 2264–2270.

9 A. B. Kaul, Two-dimensional layered materials: structure, properties, and prospects for device applications, *J. Mater. Res.*, 2014, **29**, 348–361.

10 J. Ji, X. Song, J. Liu, Z. Yan, C. Huo, S. Zhang, M. Su, L. Liao, W. Wang, Z. Ni, Y. Hao and H. Zeng, Two-dimensional antimonene single crystals grown by van der Waals epitaxy, *Nat. Commun.*, 2016, **7**, 13352.

11 S. Zhang, Z. Yan, Y. Li, Z. Chen and H. Zeng, Atomically thin arsenene and antimonene: semimetal-semiconductor and Indirect-Direct Band-Gap transitions, *Angew. Chem., Int. Ed.*, 2015, **54**(10), 3112–3115.

12 K. F. Mak, C. Lee, J. Hone, J. Shan and T. F. Heinz, Atomically thin MoS_2: A new direct-gap semiconductor, *Phys. Rev. Lett.*, 2010, **105**(13), 136805.

13 B. Radisavljevic, A. Radenovic, J. Brivio, V. Giacometti and A. Kis, Single-layer MoS_2 transistors, *Nat. Nanotechnol.*, 2011, **6**(3), 147–150.

14 A. Chernikov, C. Ruppert, H. M. Hill, A. F. Rigosi and T. F. Heinz, Population inversion and giant bandgap renormalization in atomically thin WS_2 layers, *Nat. Photonics*, 2015, **9**(7), 466–470.

15 Ł. Kłopotowski, C. Backes, A. A. Mitioglu, V. Vega-Mayoral, D. Hanlon, J. N. Coleman, V. Y. Ivanov, D. K. Maude and P. Plochocka, Revealing the nature of excitons in liquid exfoliated monolayer tungsten disulphide, *Nanotechnology*, 2016, **27**(42), 425701.

16 C. Backes, R. J. Smith, N. McEvoy, N. C. Berner, D. McCloskey, H. C. Nerl, A. O'Neill, P. J. King, T. Higgins, D. Hanlon, N. Scheuschner, J. Maultzsch, L. Houben, G. S. Duesberg, J. F. Donegan, V. Nicolosi and J. N. Coleman, Edge and confinement effects allow *in situ* measurement of size and thickness of liquid-exfoliated nanosheets, *Nat. Commun.*, 2014, **5**, 4576.

17 C. Backes, B. M. Szydłowska, A. Harvey, S. Yuan, V. Vega-Mayoral, B. R. Davies, P.-l. Zhao, D. Hanlon, E. J. G. Santos, M. I. Katsnelson, W. J. Blau, C. Gadermaier and J. N. Coleman, Production of highly monolayer enriched dispersions of liquid-exfoliated nanosheets by liquid cascade centrifugation, *ACS Nano*, 2016, **10**(1), 1589–1601.

18 H. Shi, R. Yan, S. Bertolazzi, J. Brivio, B. Gao, A. Kis, D. Jena, H. G. Xing and L. Huang, Exciton dynamics in suspended monolayer and few-layer MoS_2 2D crystals, *ACS Nano*, 2013, **7**(2), 1072–1080.

19 J. N. Coleman, M. Lotya, A. O'Neill, S. D. Bergin, P. J. King, U. Khan, K. Young, A. Gaucher, S. De, R. J. Smith, I. V. Shvets, S. K. Arora, G. Stanton, H.-Y. Kim, K. Lee, G. T. Kim, G. S. Duesberg, T. Hallam, J. J. Boland, J. J. Wang, J. F. Donegan, J. C. Grunlan, G. Moriarty, A. Shmeliov, R. J. Nicholls, J. M. Perkins, E. M. Grieveson, K. Theuwissen, D. W. McComb, P. D. Nellist and V. Nicolosi, Two-dimensional nanosheets produced by liquid exfoliation of layered materials, *Science*, 2011, **331**(6017), 568–571.

20 G. Cunningham, M. Lotya, C. S. Cucinotta, S. Sanvito, S. D. Bergin, R. Menzel, M. S. P. Shaffer and J. N. Coleman, Solvent exfoliation of transition metal dichalcogenides: Dispersibility of exfoliated nanosheets varies only weakly between compounds, *ACS Nano*, 2012, **6**(4), 3468–3480.

21 R. J. Smith, P. J. King, M. Lotya, C. Wirtz, U. Khan, S. De, A. O'Neill, G. S. Duesberg, J. C. Grunlan, G. Moriarty, J. Chen, J. Wang, A. I. Minett, V. Nicolosi and J. N. Coleman, Large-Scale exfoliation of inorganic layered compounds in aqueous surfactant solutions, *Adv. Mater.*, 2011, **23**(34), 3944–3948.

22 V. Nicolosi, M. Chhowalla, M. G. Kanatzidis, M. S. Strano and J. N. Coleman, Liquid exfoliation of layered materials, *Science*, 2013, **340**(6139), 1226419.

23 M. Chhowalla, H. S. Shin, G. Eda, L.-J. Li, K. P. Loh and H. Zhang, The chemistry of two-dimensional layered transition metal dichalcogenide nanosheets, *Nat. Chem.*, 2013, **5**(4), 263–275.

24 J. Li, M. M. Naiini, S. Vaziri, M. C. Lemme and M. Östling, Inkjet printing of MoS_2, *Adv. Funct. Mater.*, 2014, **24**(41), 6524–6531.

25 G. Eda, H. Yamaguchi, D. Voiry, T. Fujita, M. Chen and M. Chhowalla, Photoluminescence from chemically exfoliated MoS_2, *Nano Lett.*, 2011, **11**(12), 5111–5116.

26 Y. Li, A. Chernikov, X. Zhang, A. Rigosi, H. M. Hill, A. M. van der Zande, D. A. Chenet, E.-M. Shih, J. Hone and T. F. Heinz, Measurement of the optical dielectric function of monolayer transition-metal dichalcogenides: MoS_2, $MoSe_2$, WS_2, and WSe_2, *Phys. Rev. B: Condens. Matter Mater. Phys.*, 2014, **90**(20), 205422.

27 A. R. Klots, A. K. M. Newaz, B. Wang, D. Prasai, H. Krzyzanowska, J. Lin, D. Caudel, N. J. Ghimire, J. Yan, B. L. Ivanov, K. A. Velizhanin, A. Burger, D. G. Mandrus, N. H. Tolk, S. T. Pantelides and K. I. Bolotin, Probing excitonic states in suspended two-dimensional semiconductors by photocurrent spectroscopy, *Sci. Rep.*, 2014, **4**, 6608.

28 J. Tauc and A. Menth, States in the gap, *J. Non-Cryst. Solids*, 1972, **8–10**, 569–585.

29 S. Chaguetmi, F. Mammeri, S. Nowak, P. Decorse, H. Lecoq, M. Gaceur, J. Ben Naceur, S. Achour, R. Chtourou and S. Ammar, Photocatalytic activity of TiO_2 nanofibers sensitized with ZnS quantum dots, *RSC Adv.*, 2013, **3**(8), 2572.

30 N. Ghobadi, Band gap determination using absorption spectrum fitting procedure, *Int. Nano Lett.*, 2013, **3**(1), 2.

31 N. Chopra, A. Mansingh and G. K. Chadha, Electrical, optical and structural properties of amorphous V_2O_5 TeO_2 blown films, *J. Non-Cryst. Solids*, 1990, **194**, 126.

32 A. H. Woomer, T. W. Farnsworth, J. Hu, R. A. Wells, C. L. Donley and S. C. Warren, Phosphorene: synthesis,

scale-up, and quantitative optical spectroscopy, *ACS Nano*, 2015, **9**(9), 8869–8884.

33 X. Song, J. Hu and H. Zeng, Two-dimensional semiconductors: recent progress and future perspectives, *J. Mater. Chem. C*, 2013, **1**(17), 2952–2969.

34 W. Zhao, Z. Ghorannevis, L. Chu, M. Toh, C. Kloc, P. H. Tan and G. Eda, Evolution of Electronic Structure in Atomically Thin Sheets of WS_2 and WSe_2, *ACS Nano*, 2013, **7**(1), 791–797.

35 F. Consadori and R. F. Frindt, Crystal Size Effects on the Exciton Absorption Spectrum of WSe_2, *Phys. Rev. B: Solid State*, 1970, **2**, 4893–4896.

36 A. Splendiani, L. Sun, Y. Zhang, T. Li, J. Kim, C.-Y. Chim, G. Galli and F. Wang, Emerging Photoluminescence in Monolayer MoS_2, *Nano Lett.*, 2010, **10**, 1271–1275.

37 S. Gao, Y. Liang, C. D. Spataru and L. Yang, Dynamical excitonic effects in doped two-dimensional semiconductors, *Nano Lett.*, 2016, **16**, 5568–5573.

38 D. Prasai, A. R. Klots, A. K. M. Newaz, J. S. Niezgoda, N. J. Orfield, C. A. Escobar, A. Wynn, A. Efimov, G. K. Jennings, S. J. Rosenthal and K. I. Bolotin, Electrical control of near-field energy transfer between quantum dots and two-dimensional semiconductors, *Nano Lett.*, 2015, **15**, 4374–4380.

39 E. M. Y. Lee, W. A. Tisdale and A. P. Willard, Can disorder enhance incoherent exciton diffusion? *J. Phys. Chem. B*, 2015, **119**(30), 9501–9509.

40 M. Bernardi, C. Ataca, M. Palummo and J. C. Grossman, Optical and electronic properties of Two-Dimensional layered materials, *Nanophotonics*, 2017, **6**(2), 479–493.

41 J. Coleman, Liquid exfoliation of defect-free graphene, *Acc. Chem. Res.*, 2013, **46**, 14–22.

42 T. Liang, W. Sun and M. Tian, Surface tension and screen printing precision, *Chin. Sci. Bull.*, 1996, **41**, 1930–1935.

43 S. Mouri, Y. Miyauchi and K. Matsuda, Tunable Photoluminescence of monolayr MoS_2 *via* chemical doping, *Nano Lett.*, 2013, **13**, 5944–5948.

44 T. Roy, M. Tosun, X. Cao, H. Fang, D.-H. Lien, P. Zhao, Y.-Z. Chen, Y.-L. Chueh, J. Guo and A. Javey, Dual-gated MoS_2/WSe_2 van der Waals tunnel diodes and transistors, *ACS Nano*, 2015, **9**(2), 2071–2079.

45 R. T. Tung, Recent advances in Schottky barrier concepts, *Mater. Sci. Eng., R*, 2001, **35**(1), 1–138.

46 Y. Guo, Y. Han, J. Li, A. Xiang, X. Wei, S. Gao and Q. Chen, Study on the resistance distribution at the contact between molybdenum disulfide and metals, *ACS Nano*, 2014, **8**(8), 7771–7779.

47 J. Kang, W. Liu and K. Banerjee, High-performance MoS_2 transistors with low-resistance molybdenum contacts, *Appl. Phys. Lett.*, 2014, **104**(9), 093106.

48 H. Jeong, S. Bang, H. M. Oh, H. J. Jeong, S.-J. An, G. H. Han, H. Kim, K. K. Kim, J. C. Park, Y. H. Lee, G. Lerondel and M. S. Jeong, Semiconductor–insulator–semiconductor diode consisting of monolayer MoS_2, h-BN, and GaN heterostructure, *ACS Nano*, 2015, **9**(10), 10032–10038.

49 U. Mishra and J. Singh, *Semiconductor device physics and design*, Springer Science & Business Media, 2007.